AM-FM Image Analysis based on Sparse Coding Frequency Separation Approach

1st El Hadji S. Diop
Department of mathematics
University of Thies
Thies, Senegal
ehsdiop@hotmail.com

2nd Karl Skretting
ECE Department
University of Stavanger
Stavanger, Norway
karl.skretting@uis.no

3rd Abdel-O. Boudraa
IMPM Data Group
French Naval Academy IRENav
Brest, France
abdel.boudraa@ecole-navale.fr

***Abstract*—We propose here an extension to images of a sparse coding frequency separation method. The approach is based on a 2D multicomponent amplitude modulation (AM)-frequency modulation (FM) image modeling, where the 2D monocomponent parts are obtained by sparse approximations that are solved with matching pursuits. For synthetic images, a separable dictionary is built, while a patch-based dictionary learning method is adopted for real images. In fact, the total variation (TV) norm is applied on patches to select the decomposition modes with highest TV-norm, doing so yields to an interesting image analysis tool that properly separates the image frequency contents. The proposed approach turns out to share the same behaviors with the well known empirical mode decomposition (EMD) method. Obtained results are encouraging for feature and texture analysis, and for image denoising as well.**

***Index Terms*—Sparse coding, 2D AM-FM, 2D Frequency separation, Orthogonal matching pursuit.**

I. Introduction

In approximations theory, an exact signal approximation is carried out as a linear combination of a small number of vectors that are chosen from a carefully built basis. Among approximation methods, sparse solutions [1] showed up as an interesting approximation technique with efficient solvers; for example, matching pursuits [2], orthogonal MP (OMP) [3], LASSO [4] or Bregman iterations [5].

Unlike standard decomposition approaches that project data onto predefined basis functions (harmonic, wavelet), bases of the empirical mode decomposition (EMD) are derived from the data. This time domain decomposition expands in an adaptive way any real-valued signal into a reduced number of oscillating (AM-FM) components termed intrinsic mode functions (IMFs) [6]. Being fully data driven, IMFs represent the inherent temporal modes (scales) that characterize the input signal, thereby obtaining local features and their related time-frequency distribution [6]. Despite many efforts [7]–[9], EMD still encounters serious limits preventing it from correctly performing. Nonetheless, due to its flexibility to analyze nonstationary and nonlinear time series, several attempts have been started to extend it to multi-array data sets like two-dimensional (2D) data arrays and images (2D EMD) [10]–[12] being a straightforward extension of the 1D; therefore, interpolation issues are more complicated to solve. Various approaches are proposed as alternatives, by using PDEs or optimization methods [13]–[16].

AM-FM functions are of many interests in image processing, and have been widely studied [17]–[19]. We propose here the extension SCFS2 of the recent SCFS [20] to 2D. Doing so recasts 2D EMD as a 2D sparse approximation problem using a multicomponent 2D AM-FM modeling. SCFS2 models any image as a sum of modes, each being a monocomponent 2D AM-FM function approximated by SC. The tedious and time consuming 2D interpolation is now removed, it was necessary in many 2D EMD algorithms and caused the boundary side effects, undershoots, overshoots.

II. Review on 2D EMD

Extended from 1D EMD, many 2D EMD extensions of an image $I(x,y)$ are built on the followings:

1) Find all the extrema of $I(x,y)$
2) Interpolate the maxima of $I(x,y)$ (*resp.* the minima of I(x,y)) and build the upper envelope $E_{max}(x,y)$ (*resp.* the lower envelope $E_{min}(x,y)$)
3) Compute: $m(x,y) = \frac{1}{2}(E_{max}(x,y) + E_{min}(x,y))$
4) Extract the detail $d(x,y) = s(x,y) - m(x,y)$.
5) Iterate on $m(x,y)$.

Many 2D EMD algorithms mainly differ in the way the extrema are interpolated to obtain upper and lower envelopes; *e.g.*, using Delaunay triangulation [21], bi-cubic splines [10] or thin plate splines [12]. 2D EMD is based on numerical simulations, and 2D IMFs are defined as functions having either one zero between two consecutive local extrema or the same number of maxima and minima. A refinement procedure called sifting process is applied on an iterative loop on steps (1)-(4) by extracting on $d(x,y)$ until $m(x,y) = 0$. A stopping criterion should be applied to guarantee enough physical AM and FM sense for 2D IMFs; *e.g.*, based on the number of iterations [21]. Thus, I is decomposed as: $I(x,y) = \sum_{k=1}^{K} d_k(x,y) + r(x,y)$, d_k being the k^{th} 2D IMF and $r(x,y)$ the residual.

III. Proposed 2D sparse coding approach

A multicomponent 2D AM-FM image modeling is given:

$$I(x,y) = \sum_{k=0}^{K-1} a_k(x,y)\cos[\phi_k(x,y)] = \sum_{k=0}^{K-1} I_k(x,y). \quad (1)$$

$\forall\ k = 0, \cdots, K-1$, $(a_k, \nabla\phi_k)_k$ is the modulation domain representing the instantaneous AM and FM components. In 2D EMD, $I_k(x,y)$ correspond to 2D IMFs; each 2D IMF being a monocomponent narrow band 2D AM-FM image.

Let $s[m,n], \quad m \in 0,1,\ldots,M-1 \quad n \in 0,1,\ldots,N-1$ be a sampled 2D signal and D a given dictionary; D is here a set of K elements $\{d_k\}_{k=0}^{K-1}$, each element of D is commonly called (dictionary) atom and is in the 2D case a MxN matrix. The set D is assumed to be full-rank, *i.e.*, the atoms span on the space $\mathbb{R}^{M\times N}$. If one has:

$$s = \sum_{k=0}^{K-1} \alpha_k d_k = D\alpha, \quad (2)$$

then, in a dictionary learning view, (2) can be interpreted as a representation of the signal s by the coefficients $\alpha \in \mathbb{R}^K$ under the dictionary D. There is a slight misuse of matrix notation on right side of (2); D is a three-dimensional matrix (tensor) with elements $D_{m,n,k}$ and α a one-dimensional vector with elements α_k and their "product" is taken along last dimension of D and gives a MxN matrix. A common alternative notation is to let each image (block) and each atom be reshaped into a column vector of length MN.

Let us now choose discrete cosine transform (DCT) atoms for D, and set $k = i + jM, \quad i \in 0,1,\ldots,M-1 \quad j \in 0,1,\ldots,N-1$. Thus, $k \in 1,2,\ldots,MN-1$, each atom d_k is separable and defined as an outer product of two one-dimensional vectors:

$$d_k = (d_i^M)\cdot(d_j^N)^T, \quad (3)$$

where (d_i^M) and (d_j^N) are the i^{th} and j^{th} 1D DCT synthesis vectors of lengths M and N, respectively. The orthogonal 2D DCT can easily be extended to a 2D overcomplete separable dictionary by letting $\{(d_i^M)\}_i$ or $\{(d_j^N)\}_j$ or both be overcomplete 1D dictionaries. Thus, using a separable dictionary for the image $I(x,y)$ yields the multicomponent 2D AM-FM representations (1).

A. Problem statement

For $1 \le p < \infty$, let $\|\cdot\|$ be the l^p norm of any vector $v \in \mathbb{R}^N$ given as $\|v\|_p = \left(\sum_{n=1}^{N} |v[n]|^p\right)^{\frac{1}{p}}$. Let us adopt the notation *s.t.* each MxN image block and the same sized atoms are reshaped into an MN column vectors, then, let $D = \{d_k\}_k \in \mathbb{R}^{MN\times K}$ be a given dictionary. Our goal is to represent the image $I = I[k,l]$ as a linear combination of the dictionary atoms $I \approx D\alpha = \sum_{n=1}^{N} d_n\alpha_n$, *s.t.* most elements of $\alpha = (\alpha_k)_k \in \mathbb{R}^K$ are zero. In addition, such an approximation should be optimal in the sense that the reconstruction error $I - D\alpha$ is minimal in l^2 norm $\|\cdot\|$. The problem is thus formulated as follow:

$$\alpha^\star = \underset{\alpha\in\mathbb{R}^K}{\operatorname{argmin}} \frac{1}{2}\|I - D\alpha\|_2^2 \ s.t.\ \|\alpha\|_p \le s_p, \quad (4)$$

where s_p is the sparseness measure on α given in terms of l^p norm. Using a Lagrange multiplier, (4) is equivalent to:

$$\alpha^\star = \underset{\alpha\in\mathbb{R}^K}{\operatorname{argmin}} \frac{1}{2}\|I - D\alpha\|_2^2 + \lambda\|\alpha\|_p, \quad (5)$$

where $\lambda > 0$ is a tuning parameter. Using common notation, we denote $\|\alpha\|_0$ the number of nonzero elements [22] in α; *i.e.*, $\|\alpha\|_0 = \sum_{k=1}^{K}(\alpha_k \neq 0)$. For $p = 0$, equation (5) yields:

$$\alpha^\star = \underset{\alpha\in\mathbb{R}^K}{\operatorname{argmin}} \frac{1}{2}\|I - D\alpha\|_2^2 + \lambda\|\alpha\|_0. \quad (6)$$

Equation (6) is nonconvex and well known as a NP-hard problem for finding a solution. Different strategies have been developed to efficiently solve it; for instance, greedy algorithms like MP or OMP. In addition to more sparse solutions, OMP demonstrates improvements on MP as for each iteration the residual is orthogonalized onto the space spanned by the selected atoms. Indeed, an update of the coefficients of all selected dictionary atoms is performed by means of an orthogonal projection of the signal onto such selected atoms. This procedure alleviates the issue of selecting an atom more than once as in MP, which reduces MP's performance. In addition, the way coefficients are selected guarantees OMP convergence [3].

B. Proposed algorithm

The key ideas of our approach rely on a multicomponent 2D AM-FM representation of an image $I(x,y)$ (1), each monocomponent $I_k(x,y)$ is obtained by SC (6). For simple (synthetic) images, D could be known; *e.g.*, by using a separable dictionary of sines/cosines. Since real images are more complex and image features cannot be efficiently represented by sine dictionary, we propose to learn it prior to solve (6). Several dictionary learning (DL) methods have been proposed in the last decades [23]–[26]. Many of them start with an initial dictionary, and then, gradually adapt it using a set of training vectors. One popular DL approach is the online DL (ODL) [25]. Compared with other approaches [23], [24], ODL's main advantage also shared with [26], is the fact that each iteration can process only a single training vector or a mini-batch of training vectors from the possible huge set of available training vectors. This means that the dictionary is updated more frequently, and thus, converges faster to a local minimum of the objective function. Also, it has been shown that an appropriate selection of the learning rate makes the dictionary converge to a better solution than full batch methods. A dictionary for images can be learned from a set of training images by using a large set of training patches from these images, *i.e.*, small image blocks typically of size 8x8 or 16x16, patches may overlap. The initial dictionary may

be the first K training patches. In each iteration, a mini-batch of L patches is used and reshaped into L training vectors of length N, represented as columns in a matrix X (of size NxL). Afterwards, a sparse approximation of each of these vectors is found using OMP or LARS given the sparse coefficient matrix W (of size KxL), its columns are denoted α in ODL [25]. Two internal matrices are updated at iteration t, as: $A_t = \beta A_{t-1} + WW'$ and $B_t = \beta B_{t-1} + XW'$. The initial values for matrices A_t and B_t could be the KxK identity matrix and the K training vectors used for the initial dictionary. At the end of each iteration, the columns (atoms) of the dictionary is updated one by one using the gradient descent method; atom j is set to the restricted length or normalized version of vector u_j, with $u_j = d_j + (b_j - Da_j)/A_{jj}$; d_j, a_j and b_j being the j^{th} column of matrices D, A and B, respectively.

To keep the philosophy of 2D EMD where 2D IMFs are sorted from fine to coarse, each $I_k(x, y)$ is also sorted. The sorting was based on the instantaneous frequencies [20]. For images, such information is not as much relevant as in 1D. The AM component captures the local texture contrast, that is the disparity in intensity between the brightest and darkest elements of the local texture pattern, while the FM tells us about the local texture orientation, the image granularity and edges [19]. Also, 2D EMD behaves like a filterbank and a multiscale image analysis tool [13], meaning that the first decomposition mode should hold most of the intrinsic image features which will less and less appear in other modes. Due to these and since TV-norm controls both the size of image jumps and the geometry of edges, TV-norm appears to be adequate for the sorting:

$$TV(I) = \int |\nabla I|, \tag{7}$$

applied on patches. The SCFS2 is presented in Algorithm 1.

Algorithm 1: SCFS2 algorithm.

Input : I, D and λ.
Output: 2D Decomposition modes $y = (y_i)_{i=1}^M$.

Sparse coding: compute using OMP

$$\alpha^\star := \underset{\alpha \in \mathbb{R}^K}{\operatorname{argmin}} \frac{1}{2}\|I - D\alpha\|_2^2 + \lambda\|\alpha\|_0.$$

foreach *patch* l **do**
  Set $M_l = \sharp(\alpha_k \neq 0)$.
  foreach $m_l = 1$ *to* M **do**
    $y_{m_l} \leftarrow d_{m_l}\alpha_{m_l}$
    Compute the TV norm (7) of y_{m_l}:
  end
  Sort TV norms of y_{m_l} in descending order.
end
Set $y = (y_i)_{i=1}^M$ accordingly.

TABLE I
ERRORS BETWEEN MODES AND HF/LF, AND TRUE AND RECOVERED IMAGES.

	SCFS2	IEMD	Prony	Curvature
MSE(I_1, Mode$_1$)	0.65	(9.8).10^{-3}	0.66	0.88
$\|I_1 - \text{Mode}_1\|_2$	55.8	3.96	42.5	67.8
MSE(I_2, Mode$_2$)	5.3	0.13	5.54	0.24
$\|I_2 - \text{Mode}_2\|_2$	166.64	25.33	175.06	24.56
MSE($I, \hat{I}$)	5.95	1	4.9	0.7
$\|\hat{I} - I\|_2$	166.5	75	161.4	54.8

IV. EXPERIMENTS

We refer to as Modes the decomposition modes carried out with SCFS2. Results are evaluated both qualitatively and quantitatively, and compared to the existing state-of-the-art methods; namely, IEMD [12] whose decomposition modes are referred to as IMFs, approach [14] denoted here Prony-EMD and its modes referred to as P-IMFs, and curv-EMD [16] whose modes are referred to as C-Modes. For the quantitative evaluation, we use the l^2 norm $\|\cdot\|_2$, the mean squared error (MSE) and the image quality index (Q) [27] computed within a 4x4 window for a more accurate analysis. Q ranges from -1, the worst case, to 1, the perfect fit.

We first consider the synthetic image: $I(x, y) = 2\cos(2\pi\rho_1 \cos(\theta_1)x)\cos(2\pi\rho_1 \sin(\theta_1)y) + 5\cos(2\pi\rho_2 \cos(\theta_2)x)\cos(2\pi\rho_2 \sin(\theta_2)y)$, where $\rho_1 < \rho_2$ and $\theta_1 > \theta_2$. Denote I_1 and I_2 the high frequency (HF) and low frequency (LF) components, respectively. We expect the first and second decomposition modes of either approach be HF (I_1) and LF (I_2), respectively. Its decomposition is shown in Fig. 1; D is built as separable cosines. The analysis of qualitative (Fig. 1) and quantitative results (Table I) shows that the best results are obtained with SCFS2 and IEMD.

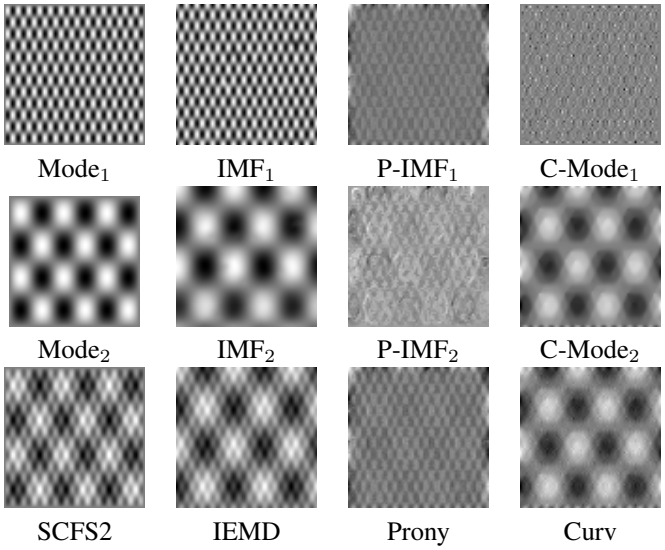

Fig. 1. Decomposition of the synthetic image.

SCFS2 is also applied on the real images, D is learned as detailed in Section III-B. Decomposition results are displayed in Figs. 3 and 4. We show above the SCFS2's capability to

TABLE II
ERRORS BETWEEN ORIGINAL AND RECOVERED IMAGES

Algorithms		L^2 norm	MSE	Q
Texture	SCFS2	0.64	$(7.7).10^{-4}$	0.9991
	IEMD	$(9.6).10^{-16}$	$(3.6).10^{-33}$	1
	Prony	5.29	0.22	0.39
	Curvature	$(1.5).10^{-15}$	$(8.2).10^{-33}$	1
Lena	SCFS2	0.67	$(1.3).10^{-3}$	0.9944
	IEMD	$(8.8).10^{-16}$	$(3.3).10^{-33}$	1
	Prony	4.18	$(2.1).10^{-2}$	0.90
	Curvature	$(3.5).10^{-15}$	$(1.3).10^{-32}$	1

properly separate the different synthetic image frequencies, this explains its multiscale property. For the Texture image (Fig. 3), one sees how the patterns are analyzed by SCFS2 through scales (order of Modes). Indeed, Mode_1 holds most of the HF (main patterns), and as the number of Modes increases; *i.e.*, Mode_k, $k > 1$, such features less appear. This is also true for other methods; however, such features are not relevant anymore for IMF_k (IEMD), P-IMF_k (Prony-EMD), $k > 2$; expect for C-Modes (curv-EMD). The same remarks hold for Lena (Figs. 4). Another benefit of SCFS2 is the fact that very fine scales are considered, compared to Curv-EMD. Finally, SCFS2 recoveries are pretty good by analyzing both the qualitative (last lines in Figs. 3 and 4) and quantitative results (Table II).

Texture Lena Noisy Lena

Fig. 2. Real images.

Next, we show an application of SCFS2 on image denoising, where the original Lena image is corrupted with a gaussian noise with a signal-to-noise ratio equal to 13.72 db, see Fig. 2. Image recoveries using SCFS2, IEMD, Prony and Curv-EMD are shown in Fig. 5. For IEMD, the first decomposition mode is exactly the noisy image, while other modes are equal to 0. For Prony and Curv-EMD, decomposition results are not far from what are displayed in Fig. 4 with some noise on modes. The noise robustness of Curv-EMD could be an interesting property, but not in the context of image denoising.

Quantitative results presented in Table III are obtained by computing errors between uncorrupted Lena image (middle column in Fig. 2) and recovered images using SCFS2, IEMD, Prony and Curv-EMD (Fig. 5).

V. CONCLUSION

The proposed extended SCFS2 method is based on a 2D multicomponent AM-FM image modeling, where the 2D monocomponent parts are carried out by SC solved with OMP. Obtained decomposition modes are sorted by applying the TV-norm on patches, yielding an interesting tool that properly separates image frequency contents. SCFS2 shows similar behaviors, neat improvements and contributions on mathematical foundations of 2D EMD. Results are encouraging for features and texture analysis, and image denoising.

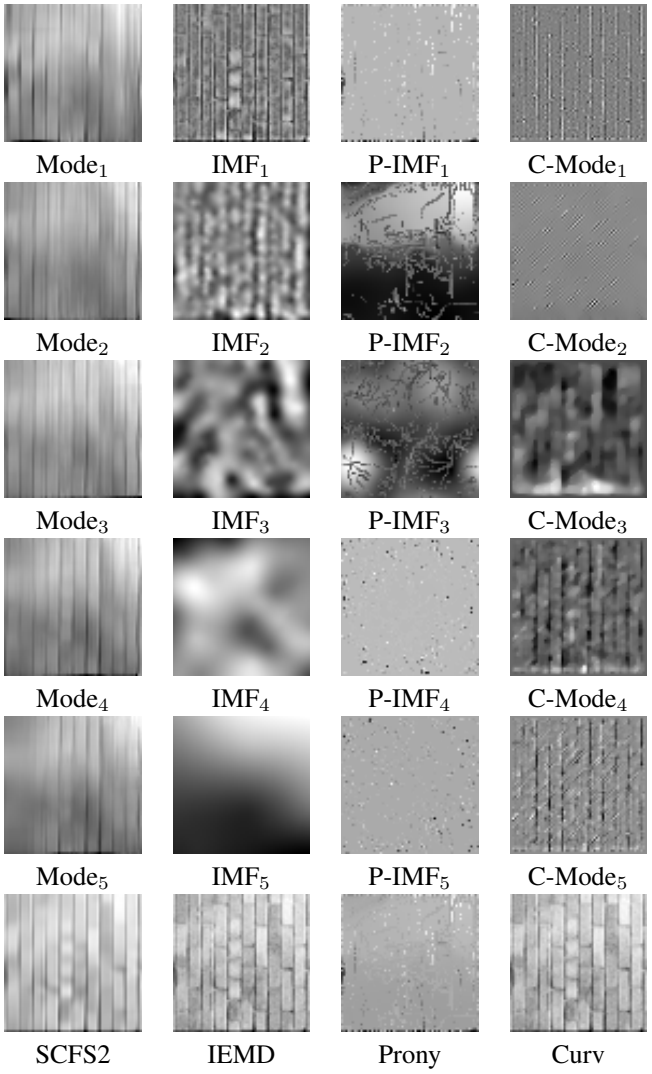

Fig. 3. Texture decomposition and image recoveries.

TABLE III
ERRORS BETWEEN ORIGINAL AND RECOVERED NOISY IMAGES

Algorithms		L^2 norm	MSE	Q
Noisy Lena	SCFS2	1.5718	$(3.63).10^{-3}$	0.98
	IEMD	1.5434	$(4.47).10^{-3}$	0.97
	Prony	5.3121	$(2.7)^{-2}$	0.88
	Curvature	1.5434	$(4.47).10^{-3}$	0.97

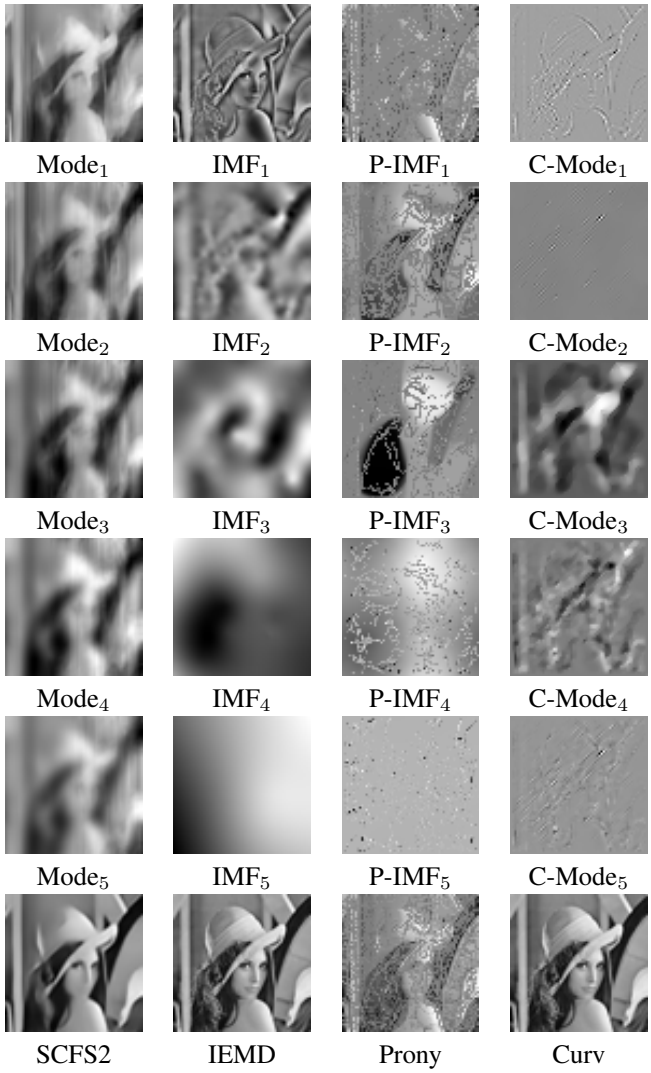

Fig. 4. Lena decomposition and image recoveries.

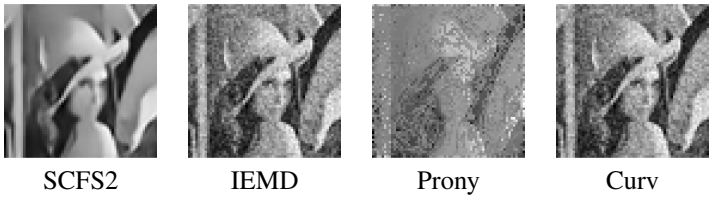

Fig. 5. Noisy Lena image recoveries.

REFERENCES

[1] M. Elad, *Sparse and redundant representations*. Springer New York, 2010.

[2] S. G. Mallat and Z. Zhang, "Matching pursuits with time-frequency dictionaries," *IEEE TSP*, vol. 41, no. 12, pp. 3397–3415, Dec. 1993.

[3] J. A. Tropp and A. C. Gilbert, "Signal Recovery From Random Measurements Via Orthogonal Matching Pursuit," *IEEE TIT*, vol. 53, no. 12, pp. 4655–4666, 2007.

[4] R. Tibshirani, "Regression shrinkage and selection via the lasso," *JRSS.*, vol. 58, no. 1, pp. 267–288, 1996.

[5] Y. Isaac, Q. Barthélemy, C. Gouy-Pailler, M. Sebag, and J. Atif, "Multi-dimensional signal approximation with sparse structured priors using split Bregman iterations," *IEE TSP*, vol. 130, pp. 389–402, Jan. 2017.

[6] N. E. Huang, Z. Shen, S. R. Long, M. C. Wu, H. H. Shih, Q. Zheng, N.-C. Yen, C. C. Tung, and H. H. Liu, "The empirical mode decomposition and the Hilbert spectrum for nonlinear and non-stationary time series analysis," *The Royal Society*, vol. 454, pp. 903–995, 1998.

[7] I. Daubechies, J. Lu, and H.-T. Wu, "Synchrosqueezed wavelet transforms: An empirical mode decomposition-like tool," *ACHA*, vol. 30, no. 2, pp. 243–261, 2011.

[8] E. H. S. Diop, R. Alexandre, and V. Perrier, "A PDE based and interpolation-free framework for modeling the sifting process in a continuous domain," *Adv. Comput. Math.*, vol. 38, no. 4, pp. 801–835, dec 2011.

[9] T. Y. Hou and Z. Shi, "Extracting a shape function for a signal with intra-wave frequency modulation," *RS A*, vol. 374, no. 2065, mar 2016.

[10] Y. Xu, B. Liu, J. Liu, and S. Riemenschneider, "Two-dimensional empirical mode decomposition by finite elements," *Royal Society A*, vol. 462, pp. 3081–3096, 2006.

[11] S. M. A. Bhuiyan, R. R. Adhami, and J. F. Khan, "Fast and adaptive bidimensional empirical mode decomposition using order-statistics filter based envelope estimation," *EURASIP JASP*, vol. 2008, no. 1, 2008.

[12] A. Linderhed, "Image empirical mode decomposition: a new tool for image processing," *Advances in Adaptive Data Analysis*, vol. 01, no. 02, pp. 265–294, 2009.

[13] E. H. S. Diop, R. Alexandre, and L. Moisan, "Intrinsic nonlinear multiscale image decomposition: A 2D empirical mode decomposition-like tool," *CVIU*, vol. 116, no. 1, pp. 102–119, Jan. 2012.

[14] J. Schmitt, N. Pustelnik, P. Borgnat, P. Flandrin, and L. Condat, "2-d prony–huang transform: A new tool for 2-d spectral analysis," *IEEE Transactions on Image Processing*, vol. 23, no. 12, pp. 5233–5248, 2014.

[15] M. A. Colominas, A. Humeau-Heurtier, and G. Schlotthauer, "Orientation-independent empirical mode decomposition for images based on unconstrained optimization," *IEEE TIP*, vol. 25, pp. 2288–2297, 2016.

[16] E. H. S. Diop, R. Alexandre, and A.-O. Boudraa, "Two-Dimensional Curvature-Based Analysis of Intrinsic Mode Functions," *IEEE SPL*, vol. 25, pp. 20–24, 2018.

[17] J. P. Havlicek, D. S. Harding, and A. C. Bovik, "Multiple dimensional quasi-eigenfunction approximations and multicomponent am-fm models," *IEEE TIP*, vol. 9, no. 2, pp. 1867–1876, Feb. 2000.

[18] F. Gianfelici, G. Biagetti, P. Crippa, and C. Turchetti, "Multicomponent AM-FM Representations: An Asymptotically Exact Approach," *IEEE Transactions on Audio, Speech and Language Processing*, vol. 15, no. 3, pp. 823–837, mar 2007.

[19] E. H. S. Diop, A. O. Boudraa, and F. Salzenstein, "A joint 2D AM–FM estimation based on higher order Teager–Kaiser energy operators," *Signal, Image and Video Processing*, vol. 5, no. 1, pp. 61–68, Mar. 2011.

[20] E. H. S. Diop and K. Skretting, "Frequency Separation Method Based on Sparse Coding," in *IEEE ICASSP*, Brighton, UK, May 2019, pp. 5192–5196.

[21] C. Damerval, S. Meignen, and V. Perrier, "A Fast Algorithm for Bidimensional EMD," *IEEE SPL*, vol. 12, no. 10, pp. 701–704, October 2005.

[22] S. Chen, C. F. N. Cowan, and P. M. Grant, "Orthogonal least squares learning algorithm for radial basis function networks," *IEEE Transactions on Neural Networks*, vol. 2, no. 2, pp. 302–309, Mar. 1991.

[23] K. Engan, S. O. Aase, and J. H. Husoy, "Frame based Signal Compression using Method of Optimal Directions (MOD)," in *IEEE ISCAS*, 1999, pp. 1–4.

[24] M. Aharon, M. Elad, and A. Bruckstein, "K-SVD: An algorithm for designing overcomplete dictionaries for sparse representation," *IEEE TSP*, vol. 54, no. 11, pp. 4311–4322, nov 2006.

[25] J. Mairal, F. Bach, J. Ponce, and G. Sapiro, "Online dictionary learning for sparse coding," in *ICML*, 2009, pp. 1–8.

[26] K. Skretting and K. Engan, "Recursive least squares dictionary learning algorithm," *IEEE TSP*, vol. 58, no. 4, pp. 2121–2130, apr 2010.

[27] Z. Wang and A. C. Bovik, "A universal image quality index," *IEEE SPL*, vol. 9, no. 3, pp. 81–84, March 2002.